

Mass Outflow from the Nucleus of the Seyfert 1 Galaxy NGC 4151¹

D.M. Crenshaw² & S.B. Kraemer^{3,4}

ABSTRACT

We present an analysis of UV and optical spectra of NGC 4151 obtained at high spectral and angular resolutions with the *Hubble Space Telescope's* (HST's) Space Telescope Imaging Spectrograph (STIS). We identify a kinematic component of the emission lines that has a width of 1170 km s^{-1} (FWHM), intermediate between those from the broad and narrow (emission) line regions (BLR and NLR). We present evidence that these emission lines arise from the same gas responsible for most of the high-column UV and X-ray absorption (component “D+E”) that we see in outflow at a distance of $\sim 0.1 \text{ pc}$ from the central nucleus. The gas in this intermediate-line region (ILR) shields the NLR and has a global covering factor of ~ 0.4 , based on the observed C IV fluxes, indicating mass outflow over a large solid angle centered on the accretion disk's axis. A large transverse velocity ($v_T \gtrsim 2100 \text{ km s}^{-1}$) compared to the radial velocity centroid ($v_r = -490 \text{ km s}^{-1}$) indicates that the kinematics is dominated by rotation at this distance, but has a significant outflow component. The mass outflow rate at 0.1 pc is $\sim 0.16 M_{\odot} \text{ yr}^{-1}$, which is about 10 times the accretion rate. Based on physical conditions in the gas and dynamical considerations, models that invoke magnetocentrifugal acceleration (e.g., in an accretion-disk wind) are favored over those that rely on radiation driving or thermal expansion as the principal driving mechanism for the mass outflow.

Subject headings: galaxies: individual (NGC 4151) – galaxies: Seyfert

¹Based on observations made with the NASA/ESA Hubble Space Telescope, obtained from the Data Archive at the Space Telescope Science Institute, which is operated by the Association of Universities for Research in Astronomy, Inc., under NASA contract NAS 5-26555.

²Department of Physics and Astronomy, Georgia State University, Astronomy Offices, One Park Place South SE, Suite 700, Atlanta, GA 30303; crenshaw@chara.gsu.edu

³Institute for Astrophysics and Computational Sciences, Department of Physics, The Catholic University of America, Washington, DC 20064; kraemer@yancey.gsfc.nasa.gov

⁴Exploration of the Universe Division, Code 667, NASA's Goddard Space Flight Center, Greenbelt, MD 20771

1. Introduction

Mass outflows of ionized gas from active galactic nuclei (AGN) are detected in the form of UV and X-ray absorption lines that are intrinsic to the AGN and blueshifted with respect to the systemic velocities of their host galaxies. While the radial velocities and physical conditions of the outflows have been characterized through intensive ground- and space-based observations over the past decade, their origin(s) and means of outward acceleration are still not well understood. The most popular dynamical models invoke accretion-disk winds and one or more acceleration mechanisms, including radiation driving, thermal expansion, and/or magnetocentrifugal winds (Crenshaw, Kraemer, & George 2003, and references therein; Proga 2003; Chelouche & Netzer 2005; Everett 2005). Another possible source of the outflows is the putative obscuring torus (Krolik & Kriss 2001), although it is possible that the torus is just the outward extension of a dusty accretion-disk wind (Königl & Kartje 1994; Elitzur & Shlosman 2006).

To distinguish between the dynamical models and determine the nature and origin of the mass outflows, we need to know the locations and complete kinematics (transverse as well as radial velocities) of the intrinsic absorbers. Several in-depth studies of Seyfert galaxies, the nearest bright AGN, have placed the absorbers at distances of tenths to tens of parsecs ($\sim 100 - 10,000$ light days) from the central continuum source (i.e., accretion disk plus X-ray corona) (Crenshaw & Kraemer 2005, and references therein). On the other hand, the high-ionization broad (emission) line region (BLR) is much closer, typically at a distance of only 3 – 10 light days in these same Seyfert galaxies (Peterson et al. 2004; Metzroth et al. 2006). Furthermore, the radial velocities of the absorbers are nearly always $< 2000 \text{ km s}^{-1}$ (Crenshaw et al. 2003), whereas the BLR velocities typically extend out to at least $10,000 \text{ km s}^{-1}$. Thus, we have suggested that most of the intrinsic absorbers observed in Seyfert galaxies are located in the inner narrow (emission) line region (NLR) (Crenshaw & Kraemer 2005), based on similarities in locations and velocities, although this certainly does not rule out an origin much closer to the nucleus.

If we want to detect and characterize mass outflows close to the nucleus, the best candidate is probably NGC 4151, the nearest ($cz = 995 \text{ km s}^{-1}$) and apparently brightest Seyfert 1 galaxy. It’s UV spectrum shows intrinsic absorption lines, spanning a wide range in ionization (O I to N V) (Bromage et al. 1985), from a number of kinematic components that cover a large range in radial velocity centroid ($v_r = 0$ to -1600 km s^{-1}) and velocity width (FWHM = 15 to 940 km s^{-1}) (Kraemer et al. 2001). Component “D+E” ($v_r = -490$

km s⁻¹, FWHM = 435 km s⁻¹), which is a blend of two kinematic components identified by Weymann et al. (1997), dominates the absorption in the UV with its high column density. This component shows variable ionic column densities that respond to continuum changes and strong metastable C III and Fe II absorption lines (Crenshaw et al. 2000), indicating high number densities ($n_H \approx 10^{7-9}$ cm⁻³) and proximity to the nucleus (Kraemer et al. 2001).

To further explore the properties of mass outflow in NGC 4151, we obtained contemporaneous high-resolution UV and X-ray spectra in 2002 May with the *HST* Space Telescope Imaging Spectrograph (STIS), the *Far Ultraviolet Spectroscopic Explorer* (*FUSE*), and the *Chandra X-ray Observatory* (*CXO*), and retrieved additional archive spectra from these missions. We give the details of the observations and analysis in Kraemer et al. (2005, Paper I) and Kraemer et al. (2006, Paper II) for the X-ray and UV data respectively. To summarize our findings, in order to match the ionic column densities of D+E and the observed covering factors of the background continuum and line emission in the line of sight (C_{los}), we needed four physical subcomponents (D+Ea, b, c, and d) characterized by different ionization parameters (U) and hydrogen column densities (N_H), as shown in Table 1. Based on the ionization parameters and the number densities (n_H) from C III metastable absorption, we found that the D+E absorbers were only ~ 0.1 pc from the central continuum source. We also found that D+Ea, the UV absorber with the highest U and N_H , was responsible for the bulk of the X-ray absorption, although we needed to include an additional, more highly ionized component (“X-High”) to account for all of the X-ray absorption, which is also listed in Table 1. Furthermore, we found that the D+E absorbers showed strong evidence for bulk motion across the BLR. From a *CXO* spectrum in 2000 March, we found a lower U and higher N_H for D+Ea (Table 1) than in 2002 May; the latter yielded a transverse velocity of $v_T \gtrsim 2500$ km s⁻¹ (Paper I). Between 2001 April and 2002 May, we noticed a change in the C_{los} of D+Ed (Table 1), which gave $v_T \approx 2100$ km s⁻¹ (Paper II), close to the previous lower limit.

The proximity of the D+E absorbers to the central SMBH in NGC 4151 and their large transverse velocities, possibly reflecting orbital motion, suggested to us that further study of this component could lead to more insight into the connection between accretion disks and mass outflows in AGN. In particular, the gas from this component must contribute in some fashion to the emission lines, and if the contribution is significant and can be isolated, it should provide additional constraints on the geometry, kinematics, and physical conditions of the gas. In Paper II, we identified a distinct component of the He II and C IV emission lines in the STIS echelle spectra of NGC 4151 with a FWHM = 1170 km s⁻¹, which is intermediate between that of the C IV broad (FWHM $\approx 10,000$ km s⁻¹) and narrow (FWHM = 250 km s⁻¹) components. We noted that the emission from this “intermediate line region” (ILR)

was absorbed by D+E. Here, we investigate the properties of the ILR in more detail, using additional emission lines from the six epochs of STIS high-resolution echelle observation. For convenience, we list the dates of observations and continuum fluxes at 1350 Å in Table 2.

2. Analysis

The available STIS E140M spectra of NGC 4151 provide a unique opportunity to deconvolve the emission-line components of NGC 4151, due to the high spectral resolution of the grating ($R = \lambda/\Delta\lambda \approx 45,000$) and the high angular resolution of *HST*. To isolate the ILR contribution, we selected a low continuum-flux spectrum with the best signal-to-noise, which was obtained on 2000 June 15. The low state minimizes the contribution of the BLR to the profile, and the small aperture used for all of the E140M spectra ($0''.2 \times 0''.2$) minimizes the contribution from the NLR. By happenstance, there was a contemporaneous high-resolution observation of NGC 4151 on 2000 July 2 through a $52 \times 0''.2$ slit with the STIS G430M grating ($R \approx 10,000$), covering the $H\beta$ and [O III] $\lambda\lambda 4959, 5007$ lines.

We show the central regions of the emission line profiles from these observations in Figure 1. The strong blueshifted absorption in the UV resonance lines ($Ly\alpha$ and the C IV and N V doublets) is due to the high-column absorption component D+E (the other absorption components are identified in Paper II). $H\beta$ also shows strong D+E absorption in the low continuum flux state, whereas a STIS G430M spectrum obtained in a high state on 1997 July 17 shows only weak $H\beta$ absorption (Hutchings et al. 2002), consistent with the weakness or absence of UV low-ionization lines from component D+E in other high continuum states (Kraemer et al. 2001, Paper II).

Figure 1 shows that the He II $\lambda 1640$ line is unaffected by intrinsic absorption and has two distinct emission components: one from the NLR ($FWHM = 250 \text{ km s}^{-1}$) and one from the ILR ($FWHM = 1170 \text{ km s}^{-1}$). There is likely a contribution from the BLR, but it is too faint to be seen in these data and is therefore included as part of the continuum fit (spline fits over large wavelength regions). We fit the profile of He II with two Gaussians, and used these profiles as templates to determine the NLR and ILR contributions to the other lines. We also detected faint BLR components in the wings of C IV, $Ly\alpha$, and $H\beta$, and fit these with splines. To model the observed emission-line profiles, we reproduced the NLR and ILR templates from He II at the expected positions of the lines (including the doublet lines of C IV $\lambda\lambda 1548, 1551$ and N V $\lambda\lambda 1239, 1243$), retaining the same velocity widths, and scaled them in intensity until we obtained a suitable match. The fits to the NLR components were straightforward, since they are unaffected by absorption, except for that in the cores of the UV resonance lines due to the host galaxy’s disk and/or halo (components F

and F' in Weymann et al. 1997). The fits to the ILR components were also relatively easy to accomplish, relying on the observed red wings of the profiles for lines with strong blueshifted absorption. Overall, this method of template scaling provided excellent fits to the profiles.

As shown in Figure 1, the use of high spatial- and spectral-resolution STIS spectra at a low continuum state allows us to easily detect and deconvolve the ILR profiles, which are essentially symmetric around zero km s^{-1} . Inspection of the profiles and fits reveals a couple of interesting results. 1) Component D+E absorbs the emission from not only the continuum and BLR, but the ILR as well, as can be seen in all of the UV resonance lines. 2) The maximum blueshifted velocity of D+E ($\sim -1400 \text{ km s}^{-1}$) is close to the maximum velocity of the ILR, which suggests self-absorption by the ILR. Hence the ILR contribution resembles a P-Cygni profile, as seen for example in the $\text{H}\beta$ profile.

As discussed in Paper II, if the velocity width of the ILR component is due primarily to gravitational motion, similar to the case for the BLR (Peterson et al. 2004), then the FWHM of the ILR profile (1170 km s^{-1}) and the mass of the supermassive black hole ($4.1 \times 10^7 M_{\odot}$, Metzroth et al. 2006) give a distance from the ILR to the central continuum source of $\sim 0.1 \text{ pc}$. This is consistent with the distance of the D+E absorbers from the central source based on their densities and ionization parameters (Paper II).

All of the above suggests a connection between the D+E absorption and the ILR, including the possibility that the ILR emission lines originate directly from gas responsible for the D+E absorbers. To test this idea, we measured the emission-line fluxes from the ILR using the fits in Figure 1. Other UV emission lines were too weak and/or absorbed to give reliable fluxes. We determined uncertainties in the fluxes by varying the scale factors applied to each template until we obtained fits that were clearly no longer acceptable. Table 3 show the observed line ratios relative to $\text{H}\beta$, as well as reddening-corrected ratios based on the very small reddening of $E(B-V) = 0.02$ in our line of sight to the nucleus, which is entirely from our Galaxy (Crenshaw & Kraemer 2005). We present photoionization models of the line ratios in the next section.

The strong C IV line provides the best opportunity for deconvolving the emission-line components in the other five epochs of STIS echelle observations, so that we can characterize the variability in the components. The other UV lines shown in Figure 1 are noisier and more difficult to deconvolve in the other epochs, particularly in high states when there is a strong BLR contribution. An attempt to deconvolve these lines resulted in error bars that were larger than the measured variations. To determine the emission-line fluxes of the separate C IV components in the six epochs of STIS E140M observations, we followed the same procedure as above; we scaled the separate C IV BLR, ILR, and NLR templates from 2000 June 15 until we obtained matches to the observed profiles.

Figure 2 shows the light curves for the C IV emission components and the continuum flux at 1350 Å. Unsurprisingly, the narrow component remained constant to within the uncertainties, which is to be expected from emission from an extended region (constrained by the aperture to be $\sim 14 \times \sim 14$ pc in the plane of the sky and possibly larger in the line of sight). The BLR shows large amplitude C IV variations similar to those of the UV continuum (maximum/minimum flux ≈ 10), consistent with previous results from more intensive UV monitoring that indicate the BLR is small (~ 6.8 light days in diameter, Metzroth, et al. 2006) and therefore responds rapidly to continuum variations. The ILR shows a positive correlation with continuum flux as well, although it is not possible to determine a time lag from these undersampled light curves. However, the timescales of the variations do put an upper limit of ~ 140 light days (~ 0.12 pc) on the radius of the ILR (i.e., from the time interval between the third and fourth observations), consistent with the value that we derived above. Interestingly, the amplitude of the ILR light curve is significantly smaller (maximum/minimum flux ≈ 4) than that of the BLR, which may be expected from a much larger region in which the amplitude is reduced by the time-delayed response of different parts of the ILR to continuum variations (Peterson 1993).

3. Photoionization Models

In Papers I and II, we determined that D+Ea has the highest C_{los} , U , and N_H of all the UV absorbers. If this subcomponent has a non-negligible global covering factor, then it must dominate the line emission from the absorbers, and it is therefore a likely source of the ILR emission. Here, we test this hypothesis by comparing the predicted emission-line fluxes from our photoionization models of D+Ea with the observed values from the ILR.

The details of the photoionization models used for this study are given in Paper I. To summarize, the models were generated using the Beta 5 version of Cloudy (Ferland et al. 1998), which includes estimated $\Delta n=0$ dielectronic recombination (DR) rates for the M-shell states of Fe and the L-shell states of the third row elements (Kraemer, Ferland, & Gabel 2004). We assumed roughly solar elemental abundances (see Paper II) and that the absorbing gas is free of cosmic dust, consistent with our previous result that there is essentially no reddening in our line of sight to the nucleus outside of the Galaxy (Crenshaw & Kraemer 2005). As per convention, the models are parameterized in terms of U and N_H . We modeled the intrinsic spectral energy distribution as a broken power law of the form $L_\nu \propto \nu^\alpha$ as follows: $\alpha = -1.0$ for energies < 13.6 eV, $\alpha = -1.3$ over the range $13.6 \text{ eV} \leq h\nu < 0.5 \text{ keV}$, and $\alpha = -0.5$ above 0.5 keV. We included a low energy cut-off at 1.24×10^{-3} eV (1 mm) and a high energy cutoff at 100 keV. The luminosity in ionizing photons for the

2002 May epoch was $Q = 1.1 \times 10^{53}$ photons s^{-1} .

In order to determine whether D+Ea could be the source of the ILR emission, we scaled the ionization parameter from the 2002 May observation to match the lower continuum flux observed in 2000 June, which yields $U = 10^{-0.92}$. We then fixed the other parameters to the 2002 May epoch and ran a new model; we list the predicted line ratios from this model (“Low-N”) in Table 3. Overall, the correspondence between the model and observed values is quite good, considering that no attempt was made to adjust the parameters derived from the D+Ea absorber to match the ILR ratios. The low [O III]/H β ratio in particular confirms that we have the correct density (n_H).

Table 3 shows that C IV λ 1550 is slightly underpredicted and N V λ 1240 is too low by a factor of ~ 2.4 . While increasing n_H by a factor of ~ 10 brings the predicted C IV emission inside the error bars, the [O III] λ 5007 is then collisionally suppressed. This scenario would therefore require an additional component of lower density gas to provide the [O III] emission. Moreover, N V is still underpredicted at the higher density. Although strong N V emission is often cited as evidence of super-solar nitrogen abundances (e.g., Hamann et al. 2002), we find that increasing N/H in the models results in an overprediction of N IV] λ 1486/H β (the observed value is ~ 1.2 for the BLR, ILR, and NLR combined). The underprediction of N V is not unique to this case, as we have encountered it on a number of occasions when modeling the physical conditions in the NLR (e.g., Kraemer et al. 2000; Kraemer & Crenshaw 2000).

Having established that it is plausible that D+Ea is the source of the ILR emission, we generated a grid of models to determine if the observed variations in the C IV flux could result from the response of this component to changes in the strength of the ionizing continuum. As with our model of the emission line ratios, we assumed that the ionizing flux, and therefore U , scale linearly with the continuum flux at 1350 Å. Figure 3 shows that Low-N, with $N_H = 10^{22.46}$ cm^{-2} , cannot replicate the behavior of the observed C IV fluxes, as the model curve turns over too quickly, due to the fact that too much C $^{+3}$ is ionized into C $^{+4}$ at the higher flux states.

We were able to remedy this problem by increasing N_H to $10^{22.93}$ cm^{-2} , the column density of D+Ea in 2000 March (Table 1). In Table 3, we list the emission line ratios for this model (“High-N”). The differences in line ratios between the low- and high column density models are negligible. Figure 3 shows that High-N is able to reproduce the observed positive correlation of continuum and C IV ILR fluxes. Thus, we conclude that the higher column density is more appropriate globally, and that the low column in 2002 May due to transverse motion is atypical. This is consistent with our previous claim that variations in the equivalent widths of the absorption lines from D+E over the time period of the STIS echelle observations were primarily due to changes in the ionizing continuum, until the large

drop in column density seen in 2002 May (Paper II). Interestingly, we found that varying the ionization parameter for X-High suppresses F_{CIV} for the lowest values of U , which suggests that the ILR may not be fully screened by this component.

The global covering factor (C_g) of the ILR gas can be obtained from the scale factor needed to match the model curve in Figure 3 with the general trend of the observed C IV fluxes. For model High-N, we find that $C_g = 0.4$, which is significant, and yet reassuringly does not exceed one. The predicted C IV flux initially increases with continuum flux, but begins to decrease after peaking at $F(1350) = 1.3 \times 10^{-13}$ ergs cm $^{-2}$ s $^{-1}$. Thus, our highest observed C IV flux comes after the peak, and the model predicts that even higher continuum levels would result in significantly lower C IV fluxes from the ILR.

Although the High-N model matches the behavior of the ILR C IV emission reasonably well, the agreement is not perfect. We attribute these discrepancies to the size of the ILR and light travel time effects, which are difficult to disentangle since the light curves in Figure 2 are severely undersampled. For example, the most discrepant C IV flux, obtained during 2002 May, may simply be due to the fact that the higher continuum flux in our line-of-sight has yet to reach the bulk of the ILR gas, which is irradiated by weaker continuum flux from an earlier epoch as we see it. Another possible problem is that the global covering factor required for the ILR models exceeds, by a factor of ~ 4 , the constraint that we derived from the forbidden O VII 22.1 Å emission line in Paper I. A likely explanation is that most of the O VII emission is absorbed across the entire profile by the large soft X-ray opacity (primarily the He II edge) of D+Ea, whereas the UV resonance lines are only self-absorbed in part of their blue wings.

4. Summary and Discussion

We have discovered a distinct component of the emission lines in NGC 4151 that has a width (FWHM ≈ 1170 km s $^{-1}$) between those of the classic broad and narrow emission lines. We were able to isolate this component by using *HST* spectra at high spectral and angular resolutions, which reduce the contribution of the NLR to the lines, of NGC 4151 in a low continuum-flux state, which reduces the BLR contribution. This intermediate-line region (ILR) would be difficult to detect in ground-based observations, especially in moderate- to high-flux states, and its connection to previous claims of ILRs in Seyfert galaxies and quasars (e.g., Brotherton et al. 1994; cf. Sulentic & Marziani 1999) is therefore uncertain.

The properties of the ILR lead us to believe that we have found the emission from at least the major component (D+Ea) of the high-column outflowing absorbers in NGC 4151, based

on the following evidence. 1) The ILR emission and blueshifted absorption lines extend to about the same velocity range (-1400 km s^{-1}), and together they resemble P-Cygni profiles, suggesting self-absorption. 2) The approximate location of the ILR ($\sim 0.1 \text{ pc}$), derived from the width of the emission lines, is consistent with that of the D+E absorbers based on their ionization parameters and densities. 3) A photoionization model of the D+Ea absorber that is completely constrained in terms of U , N_H , and n_H gives line ratios that are close to the observed ILR values.

Given that the ILR emission lines are from the same kinematic component that produces the D+Ea absorption, the emission lines provide additional constraints on the mass outflow. Our photoionization models are able to reproduce the observed correlation of continuum and C IV fluxes in the STIS data if we use the higher column density from 2000 March ($N_H = 10^{22.93} \text{ cm}^{-2}$), as opposed to that from 2002 May ($N_H = 10^{22.5} \text{ cm}^{-2}$), suggesting that the former value is a more appropriate global average. Furthermore, the scale factor needed to match the observed ILR C IV fluxes gives us a global covering factor of $C_g = 0.4$ for the bulk of the mass outflow. This value derived for an individual Seyfert is similar to that derived from the frequency of absorbers in Seyfert galaxies, $C_g \approx 0.5$, assuming that all Seyfert 1 galaxies have mass outflows (as opposed to $\sim 50\%$ of Seyferts having outflows with $C_g = 1$, Crenshaw et al. 1999). However, we note that the D+Ea absorption in NGC 4151 has an unusually large column density and small distance from the continuum source compared to most UV absorbers (Crenshaw et al. 2003). One possible interpretation is that the majority of the mass outflow in NGC 4151 is at an early stage of evolution. Another possibility is that the high column is due to a special viewing angle, close to the edge of the NLR bicone, as discussed below.

Previous photoionization studies (Alexander et al. 1999; Kraemer et al. 2000) have concluded that the ionizing radiation incident on the NLR in NGC 4151 is filtered by absorption close to the continuum source. In Kraemer et al. (2000), we predicted an absorber with $U = 1$ and $N_H = 10^{22.5}$, which are remarkably close to the values for D+Ea and the ILR. Thus, the ILR is likely shielding the NLR, which places some interesting constraints on its geometry. Based on kinematic models of *HST* long-slit spectra of NGC 4151, we found that the velocity field of the NLR can be explained by radial outflow in a bicone with an axis inclined by $\sim 45^\circ$ with respect to our line of sight, with the outflowing gas roughly confined between inner and outer half-opening (polar) angles of $\theta = 15^\circ$ and 33° (Das et al. 2005). Although this geometry places our line of sight just outside of the bicone, we can still see the nucleus of this Seyfert 1 galaxy because the source of obscuration, and therefore the bicone edges, do not have sharp edges (Evans et al. 1993; Schmitt et al. 2006). In order to shield the NLR and be in our line of sight as well, the ILR must cover at least polar angles from 15° to 45° which yields a global covering factor of $C_g \geq 0.26$. Extending the coverage to

$\theta = 15 - 55^\circ$ increases C_g to the observed value of 0.4, whereas filling in the cone so that $\theta = 0 - 55^\circ$ increases it slightly more to 0.43. We conclude that mass outflow in the ILR covers a large solid angle that is likely focused in the polar direction. Furthermore, the high column density in our line of sight ($\theta = 45^\circ$) compared to other Seyferts that are more likely viewed pole-on, suggests that the N_H is increasing with polar angle, and assuming this trend continues, it is consistent with previous suggestions that the source of obscuration in the unified scheme is an optically thick wind more focused toward the plane of the accretion disk ($\theta = 90^\circ$) (Königl & Kartje 1994; Elitzur & Shlosman 2006).

In Papers I and II, we determined transverse velocities of the D+E absorbers that were on the order of $v_T \approx 2100 \text{ km s}^{-1}$ or larger. These values are considerably higher than the radial velocity centroid at $v_r = -490 \text{ km s}^{-1}$, which suggests that the kinematics of the gas at $\sim 0.1 \text{ pc}$ is dominated by rotation, but with a significant outflow component. A transverse velocity of 2100 km s^{-1} leads to a somewhat smaller distance ($\sim 0.04 \text{ pc}$), but that assumes purely gravitational motion at this distance, which may not be the case, as discussed below.

It is interesting that the transverse velocity of the absorber is higher than the largest emission-line radial velocity, given by the half-width at zero intensity (HWZI) of the emission lines ($\sim 1400 \text{ km s}^{-1}$), which is possible for a number of different outflow geometries. For example, in Figure 4, we show perhaps the simplest model that can satisfy our geometric and kinematic constraints. In this model, the line of sight velocity is the same as the velocity in the “r” direction (v_r), which can also be equated to the outflow velocity. For simplicity, we assume constant v_r and v_ϕ (in standard spherical coordinates) and that the flow is at a constant polar angle ($v_T = v_\phi$, $v_\theta = 0$), although in general \mathbf{v}_T is the vector sum of \mathbf{v}_ϕ and \mathbf{v}_θ . The resulting curve of motion is a spiral along a cone with a half-opening angle of $\theta = 45^\circ$. If $v_\phi = 2100 \text{ km s}^{-1}$ holds for other ILR clouds (i.e., those not seen in absorption), we calculate that the highest emission-line radial velocity in this model is 1550 km s^{-1} , which is indeed smaller than the transverse velocity and close to the observed HWZI of the ILR profile. For comparison, we also plot a curve in Figure 4 with $v_\phi = 10,000 \text{ km s}^{-1}$, which helps to show the conical surface that the clouds follows. However, this case results in emission-line velocities much higher than those seen in the ILR. Thus, at least in this simple model, v_T cannot be much higher than $\sim 2100 \text{ km s}^{-1}$.

It is easy to think of D+Ea as a cloud, as drawn in Figure 4, since the radial thickness of D+Ea is $N_H/n_H = 1.3 \times 10^{16} \text{ cm} = 0.004 \text{ pc}$, which is only $\sim 4\%$ of its radial distance from the central source. Thus, the ILR can then be thought of as a collection of “clouds” that altogether cover $\sim 40\%$ of the sky as seen from the central source. However, it could also take the form of a relatively thin (partial) shell or flow tube with column density inhomogeneities in the radial direction. The relative thickness of X-high is $\sim 30\%$ if it is near D+E (but a

smaller percentage at smaller distances), so it could be more like a semi-continuous “wind”.

Assuming that the radial velocity centroid of D+Ea is the approximate outflow velocity, the mass outflow rate due to this component is $\dot{M}_{out} = 4\pi r N_H m_H C_g v_r = 0.16 M_\odot \text{ yr}^{-1}$, where m_p is the mass of a proton. If we include the other X-ray and UV components (dominated by X-high) and assume the same C_g , the outflow rate increases to $\dot{M}_{out} = 0.19 M_\odot \text{ yr}^{-1}$. On the other hand, the inferred accretion rate is only $\dot{M}_{acc} = 0.013 M_\odot \text{ yr}^{-1}$, based on the average bolometric luminosity of NGC 4151 ($L_{bol} = 7.3 \times 10^{43} \text{ ergs s}^{-1}$, Kaspi et al. 2005) and an expected efficiency of ~ 0.1 in the conversion of mass infall to energy (Peterson 1997). This difference can be explained by one of two scenarios, or a combination of the two). 1) In a steady-state situation, most (more than 90%) of the inflowing mass at $\sim 0.1 \text{ pc}$ is not eventually accreted, but is instead driven outward, or 2) the current episode of mass ejection in NGC 4151 is an unusual or infrequent event, preceded by a long interval of mass accumulation into a reservoir (e.g., accretion disk).

In Paper I, we examined the possible dynamical forces (radiation driving, thermal expansion, magnetocentrifugal acceleration) that could possibly drive the outflow in NGC 4151. Here we review our arguments using a revised value for the black-hole mass ($M = 4.1 \times 10^7 M_\odot$, Metzroth et al. 2006), which yields an Eddington ratio of $L_{bol}/L_E = 0.014$. In order for radiation pressure to drive the gas outward from the nucleus, the force multiplier must be $FM \geq (L_{bol}/L_E)^{-1} = 71$. From our photoionization models, we found that $FM \leq 2$ for X-High, $FM \leq 41$ for D+Ea in 2002, and $FM \leq 11$ for D+Ea at historically high continuum flux levels (four times the 2002 level, see Paper I). These values are upper limits because they were calculated for the optically thin case, whereas the force multiplier decreases into a cloud as it becomes optically thick (Chelouche & Netzer 2005). Dust grains are efficient absorbers of radiation and could greatly increase the effective force multipliers, but the lack of reddening indicates that dust is essentially absent in the high-column absorbers (e.g., a Galactic dust/gas ratio would result in a reddening of $E_{B-V} \approx 16 \text{ mag}$ for D+Ea). The lack of dust is not surprising since the absorbers are near and likely originated inside the dust sublimation radius, $r_{sub} \approx 1.3 L_{46}^{1/2} T_{1500}^{-2.8} \text{ pc} \approx 0.11 \text{ pc}$ (Barvainis 1987). Thus, X-high cannot be radiatively driven and D+Ea is only marginally susceptible to radiation driving in low to medium flux states. However, we cannot rule out the possibility that the absorbers had lower U when they were closer to the central nucleus and were therefore more susceptible to radiation driving.

For a thermal wind, the radial distance at which the gas can escape is given by $r_{esc} \geq GMm_H/T_g k$ (Crenshaw et al. 2003, and references therein), where T_g is the gas temperature and k is the Boltzmann constant. Our photoionization models give $T_g = 5 \times 10^4 \text{ K}$ and $3 \times 10^6 \text{ K}$ for D+Ea and X-High, which yield $r_{esc} \geq 1.3 \times 10^{21} \text{ cm}$ and $\geq 2.2 \times 10^{19}$, respectively.

These are much greater than the radial locations of D+Ea and X-high, so these high-column components cannot be attributed to thermal winds.

An MHD flow is therefore a likely possibility, at least by comparison to the current alternatives. Accretion disk winds that invoke magnetocentrifugal acceleration (Emmering, Blandford, & Shlosman 1992; Bottorff, Korista, & Shlosman 2000) predict that the gas will flow along rotating magnetic field lines, which would result in significant transverse velocities as seen by an outside observer, as illustrated in Figure 4. In the presence of non-dissipative MHD waves, the line widths can greatly exceed the thermal widths (Bottorff et al. 2000), which could explain the large width of D+Ea ($\text{FWHM} = 450 \text{ km s}^{-1}$). Everett (2005) presents an accretion-disk wind model that incorporates both radiative and magnetocentrifugal acceleration. Further clues to the nature of mass outflows in AGN will come from comparing predictions from these models with detailed observational constraints, such as those we have presented for NGC 4151.

We thank Brad Peterson, Gary Ferland, Alvin Das, and John Everett for helpful discussions. Some of the data presented in this paper were obtained from the Multimission Archive at the Space Telescope Science Institute (MAST). STScI is operated by the Association of Universities for Research in Astronomy, Inc., under NASA contract NAS5-26555. Support for MAST for non-HST data is provided by the NASA Office of Space Science via grant NAG5-7584 and by other grants and contracts. This research has made use of the NASA/IPAC Extragalactic Database (NED) which is operated by the Jet Propulsion Laboratory, California Institute of Technology, under contract with the National Aeronautics and Space Administration.

REFERENCES

- Alexander, T., Sturm, E., Lutz, D., Sternberg, A., Netzer, H., & Genzel, R. 1999, *ApJ*, 512, 204.
- Barvainis, R. 1987, *ApJ*, 320, 537.
- Bromage, G.E., et al. 1985, *MNRAS*, 215, 1.
- Bottoff, M.C., Korista, K.T., Shlosman, I. 2000, *ApJ*, 537, 134.
- Brotherton, M.S., Wills, B.J., Francis, P.J., & Steidel, C.C. 1994, *ApJ*, 430, 495.
- Chelouche, D. & Netzer, H. 2005, *ApJ*, 625, 95.
- Crenshaw, D.M. & Kraemer, S.B. 2005, *ApJ*, 625, 680.
- Crenshaw, D.M., Kraemer, S.B., Boggess, A., Maran, S.P., Mushotzky, R.F., & Wu, C.-C. 1999, *ApJ*, 516, 750.
- Crenshaw, D.M., Kraemer, S.B., & George, I.M. 2003, *ARA&A*, 41, 117.
- Crenshaw, D.M., et al. 2000, *ApJ*, 545, L27.
- Das, V., et al. 2005, *AJ*, 130, 945.
- Emmering, R.T., Blandford, R.D., & Shlosman, I. 1992, *ApJ*, 385, 460.
- Elitzur, M. & Shlosman, I. 2006, *ApJ*, in press (astro-ph/0605686).
- Evans, I.N., Tsvetanov, Z., Kriss, G.A., Ford, H.C., Caganoff, S., & Koratkar, A.P. 1993, *ApJ*, 417, 82.
- Everett, J.E. 2005, *ApJ*, 631, 689.
- Ferland, G.J., Korista, K.T., Verner, D.A., Ferguson, J.W., Kingdon, J.B., & Verner, E.M. 1998, *PASP*, 110, 749.
- Hamann, F., Korista, K.T., Ferland, G.J., Warner, C., & Baldwin, J. 2002, *ApJ*, 564, 592.
- Hutchings, J.B., Crenshaw, D.M., Kraemer, S.B., Gabel, J.R., Kaiser, M.E., Weistrop, D., & Gull, T.R. 2002, *AJ*, 124, 2543.
- Kaspi, S., Maoz, D., Netzer, H., Peterson, B.M., Vestergaard, M., & Jannuzi, B.T. 2005, *ApJ*, 629, 61.
- Königl A., & Kartje J. 1994, *ApJ*, 424, 446.
- Kraemer, S.B. & Crenshaw, D.M. 2000, *ApJ*, 544, 763.
- Kraemer, S.B., Crenshaw, D.M., Hutchings, J.B., Gull, T.R., Kaiser, M.E., Nelson, C.H., & Weistrop, D. 2000, *ApJ*, 531, 278.
- Kraemer, S.B., Ferland, G.J., & Gable, J.R. 2004, *ApJ*, 604, 56.

- Kraemer, S.B., et al. 2001, ApJ, 551, 671.
- Kraemer, S.B., et al. 2005, ApJ, 633, 693 (Paper I).
- Kraemer, S.B., et al. 2006, ApJ, in press (astro-ph/0608383) (Paper II).
- Krolik, J.H. & Kriss, G.A. 2001, ApJ, 561, 684.
- Metzroth, K.G., Onken, C.A., & Peterson, B.M. 2006, ApJ, 647, 901.
- Peterson, B.M. 1993, PASP, 105, 247.
- Peterson, B.M. 1997, An Introduction to Active Galactic Nuclei (Cambridge, UK: Cambridge University Press).
- Peterson, B.M., et al. 2004, ApJ, 613, 682.
- Proga, D. 2003, ApJ, 585, 406.
- Schmitt, H.R., Kraemer, S.B., Crenshaw, D.M., & Hutchings, J.B. 2006, in The X-ray Universe 2005, ed. A. Wilson, ESA SP-604, 661.
- Sulentic, J.W. & Marziani, P. 1999, ApJ, 518, 9.
- Weymann, R.J., Morris, S.K., Gray, M.E., & Hutchings, J.B. 1997, ApJ, 483, 717.

Fig. 1.— Emission-line profiles from the STIS E140M observation on 2000 June 15 (top four panels) and G430M observation (bottom two panels) on 2000 July 2. The solid black line shows the observed flux as a function of radial velocity in the rest frame of NGC 4151 ($z = 0.00332$). Components of the profiles fits are: continuum + NLR (dotted blue), continuum + BLR (dotted-dashed green), continuum + BLR + ILR (dashed red), and continuum + BLR + ILR + NLR (dashed black). The full extent of absorption component D+E (including doublets) is given below the profiles. The absorption at more negative velocities in the $L\alpha$ profile is due to Galactic $L\alpha$, and the absorption in the cores of the narrow UV resonance lines is due to components F and F' from NGC 4151's ISM and halo. The slight offsets in the apparent velocities of the narrow and intermediate profiles are due to blending of the doublets and/or to different shapes and contributions of the underlying broad and continuum emissions.

Fig. 2.— Light curves of the continuum flux at 1350 Å (bottom panel, in units of 10^{-14} ergs $s^{-1} \text{ cm}^{-2} \text{ Å}^{-1}$) and the C IV emission components (top three panels, in units of 10^{-12} ergs $s^{-1} \text{ cm}^{-2}$) from the STIS E140M spectra.

Fig. 3.— The model predictions of ILR C IV flux as a function of continuum flux at 1350 Å for $N_H = 10^{22.46} \text{ cm}^{-2}$ (dotted line) and $N_H = 10^{22.93} \text{ cm}^{-2}$ (dashed line), compared to the observed fluxes. The details of the scaling of the model results are given in the text. The continuum flux is in units of ergs $s^{-1} \text{ cm}^{-2} \text{ Å}^{-1}$ and the C IV emission flux is in units of ergs $s^{-1} \text{ cm}^{-2}$.

Fig. 4.— Schematic diagram of a simple model for the geometry and kinematics of the ILR. The line of sight is in the y - z plane, at a polar angle of $\theta = 45^\circ$ from the rotation axis (z) of the accretion disk. Unit vectors for the velocity components are shown at the location of the D+Ea absorber, at a radial distance of 0.1 pc from the inner accretion disk and BLR. The solid red line shows the curve of motion for the D+Ea absorber over 1000 years assuming $v_r = 490 \text{ km s}^{-1}$, $v_\phi = 2100 \text{ km s}^{-1}$, and $v_\theta = 0$. The grey curve shows the curve of motion over the same time period for $v_r = 490 \text{ km s}^{-1}$, $v_\phi = 10,000 \text{ km s}^{-1}$, and $v_\theta = 0$. Additional ILR clouds moving in a similar fashion are assumed to cover the BLR at a distance of ~ 0.1 pc within the cone at $\theta \leq 45^\circ$, and possible extending to $\theta \approx 55^\circ$.

Table 1. NGC 4151 Absorption Components

Name	Date	C_{los}	$\log U$	$\log N_H$ (cm^{-2})	$\log n_H^a$ (cm^{-3})
X-high	2002 May	1.0	1.05	22.5	≥ 5.5
D+Ea	2002 May	0.9	-0.27	22.46	6.8
	2000 Mar	0.9	-0.57	22.93	6.8
D+Eb	2002 May	0.8	-1.67	20.8	8.1
D+Ec	2002 May	0.5	-1.08	21.6	7.4
D+Ed	2002 May	0.2	-3.1	19.5	9.5
	2001 Apr	0.7	-4.0	19.5	9.5

^aFrom profile fits to the metastable C III absorption for subcomponents a, b, and c (Paper II). The number density for D+Ed is obtained by assuming co-location with the other subcomponents, and the upper limit for X-high is derived from evidence that it is interior to D+E.

Table 2. STIS E140M Spectra of NGC 4151

UT Date	Julian Date	F(1350) ^a
1999 July 19	2,451,380	9.4
2000 March 3	2,451,607	4.3
2000 June 15	2,451,711	2.5
2000 November 5	2,451,854	17.3
2001 April 14	2,452,014	1.4
2002 May 8	2,452,403	11.3

^aUnits of 10^{-14} ergs $\text{s}^{-1} \text{cm}^{-2} \text{\AA}^{-1}$.

Table 3. NGC 4151 – ILR Line Ratios (Relative to $H\beta^a$)

Emission Line	Observed	Dereddened ^b	Model Low-N ^c	Model High-N ^d
Ly α λ 1216	41.7	46.9 \pm 13.2	42.3	39.4
N V λ 1240	6.2	6.9 \pm 1.9	2.9	2.7
C IV λ 1550	37.5	40.6 \pm 9.0	28.7	26.7
He II λ 1640	1.4	1.5 \pm 0.4	1.9	1.8
[O III] λ 5007	4.5	4.5 \pm 0.8	5.4	5.1

^aObserved flux of ILR $H\beta = 1.89 (\pm 0.32) \times 10^{-13}$ ergs s⁻¹ cm⁻²

^bFrom $E_{B-V} = 0.02$ and the standard Galactic reddening curve of Savage & Mathis (1979).

^cModel parameters: $U = 10^{-0.92}$, $N_H = 10^{22.46}$ cm⁻², and $n_H = 10^{6.75}$ cm⁻³.

^dModel parameters: $U = 10^{-0.92}$, $N_H = 10^{22.93}$ cm⁻², and $n_H = 10^{6.75}$ cm⁻³.

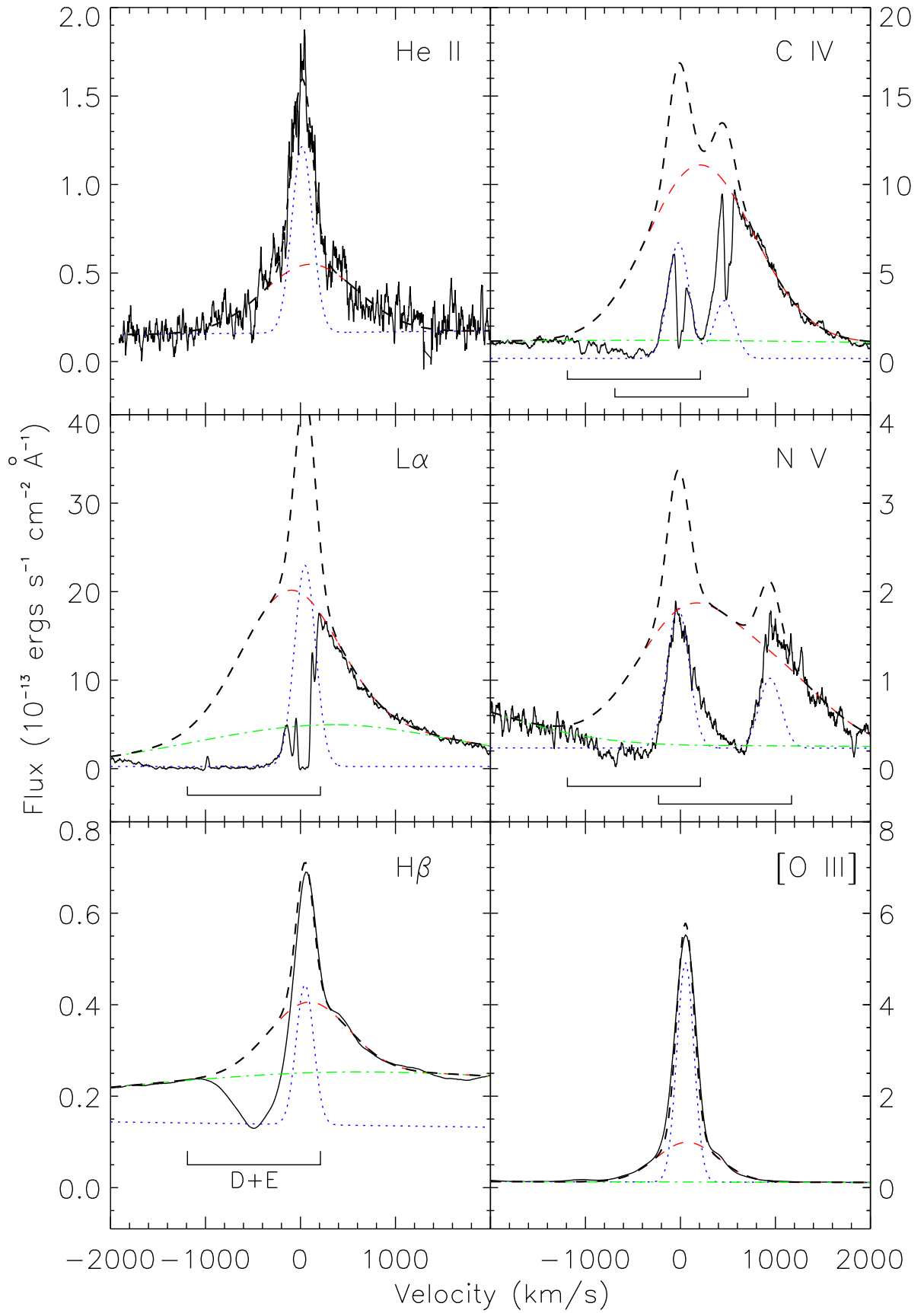


Fig. 1

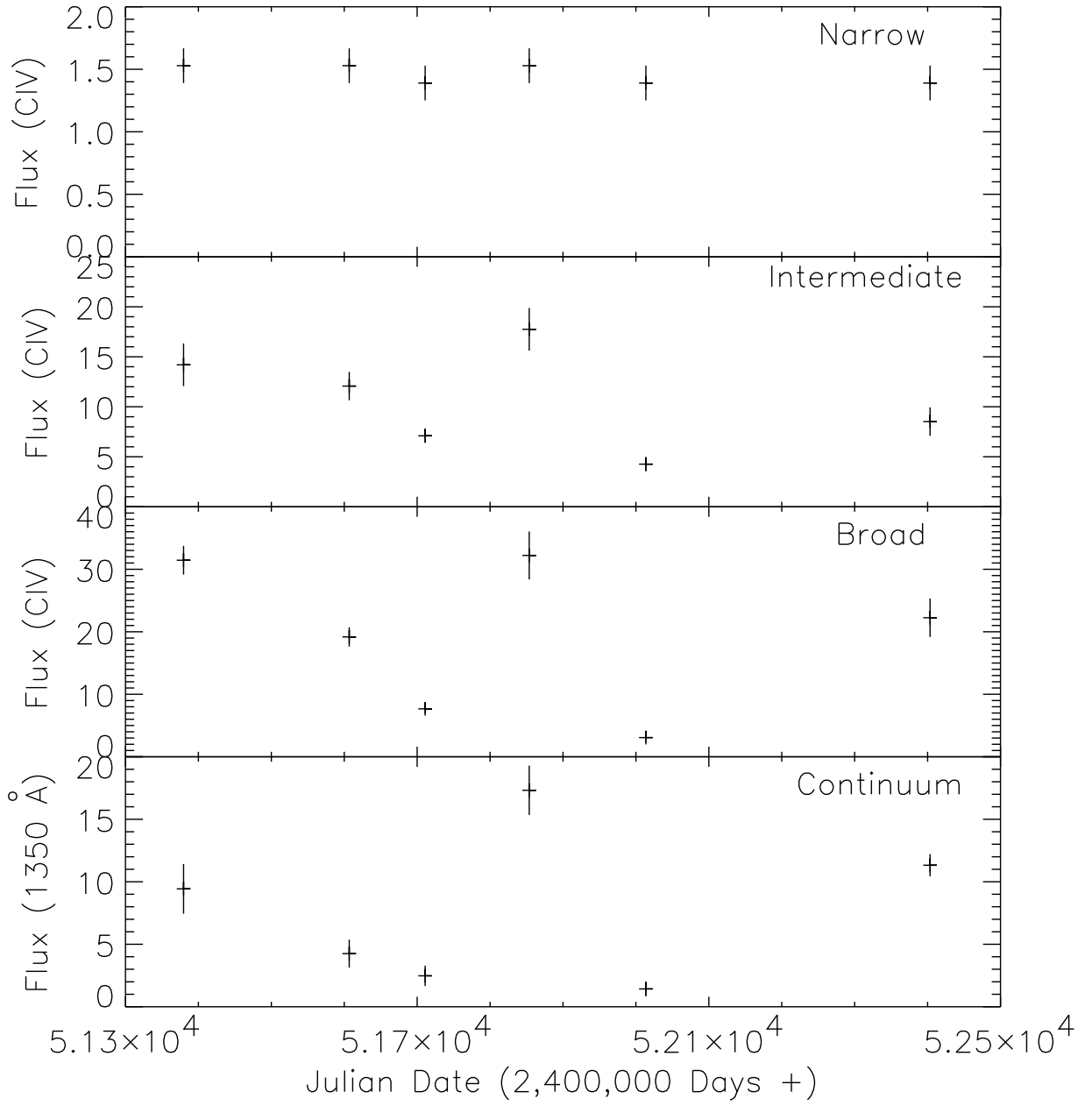


Fig. 2

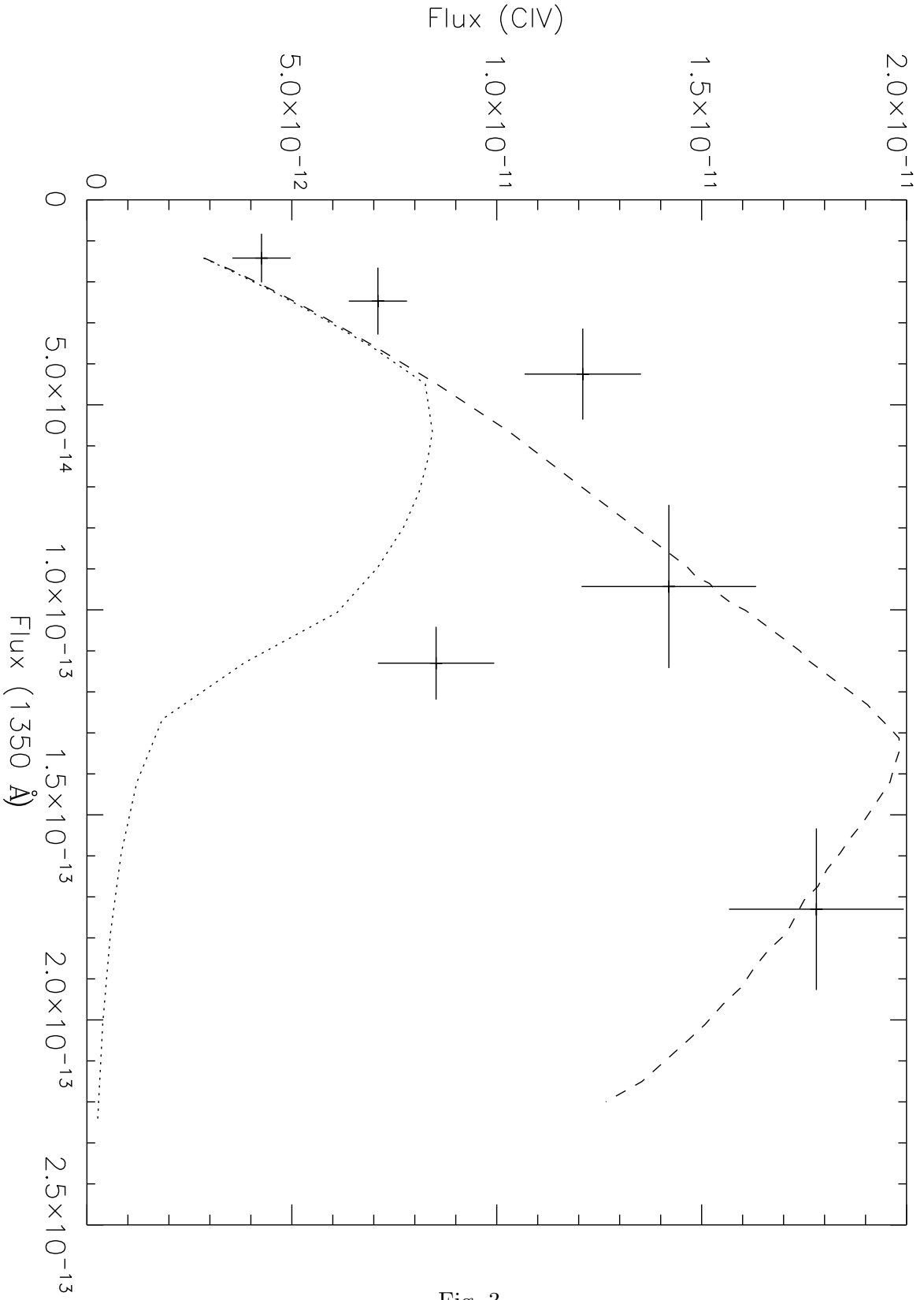


Fig. 3

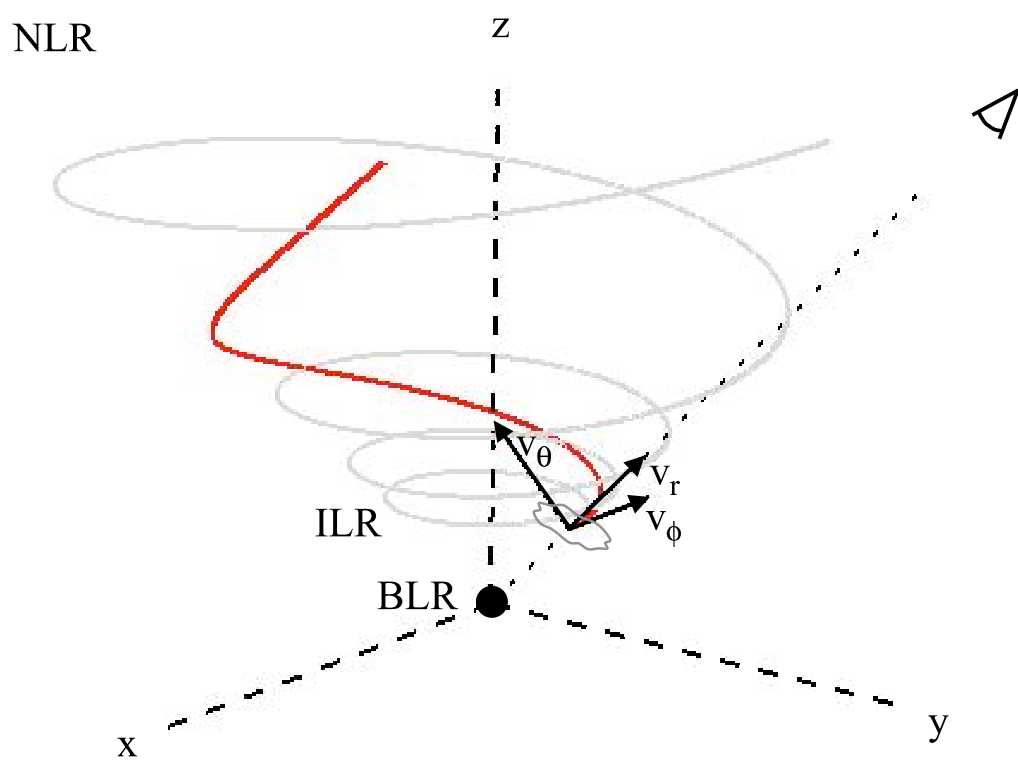


Fig. 4